Advances in Radiation Oncology (2021) 6, 100775

advances in radiation oncology

www.advancesradonc.org

Scientific Article

Evaluation of Threshold Dose of Damaged Hepatic Tissue After Carbon-Ion Radiation Therapy Using Gd-EOB-DTPA–Enhanced Magnetic Resonance Imaging

Masashi Ebara, MD,[a] Kei Shibuya, MD, PhD,[a,b,c,*] Hirofumi Shimada, PhD,[c] Motohiro Kawashima, PhD,[c] Hiromi Hirasawa, MD, PhD,[a] Ayako Taketomi-Takahashi, MD PhD,[a] Tatsuya Ohno, MD, PhD,[b,c] and Yoshito Tsushima, MD, PhD[a]

[a]*Department of Diagnostic Radiology and Nuclear Medicine, Gunma University Graduate School of Medicine, Gunma, Japan;* [b]*Department of Radiation Oncology, Gunma University Graduate School of Medicine, Gunma, Japan;* [c]*Gunma University Heavy Ion Medical Center, Gunma, Japan*

Received March 28, 2021; revised July 27, 2021; accepted August 9, 2021

Abstract

Purpose: To evaluate the threshold dose and associated factors using signal-intensity changes in the irradiated area after carbon-ion radiation therapy (C-ion RT) for patients with liver cancer.

Methods and Materials: Patients treated for the first time with C-ion RT for malignant liver tumors and followed up with 3-Tesla gadoxetic acid (Gd-EOB-DTPA)–enhanced magnetic resonance imaging (MRI) 3 months after treatment completion were retrospectively enrolled. The volume of focal liver reaction (FLR), a low-intensity area in the hepatobiliary phase of Gd-EOB-DTPA after treatment, was measured. Corrected FLR (cFLR) volume, defined as FLR corrected for changes in tumor volume from before to after treatment, was calculated, and the threshold dose was determined by applying the cFLR volume in the dose-volume histogram. To evaluate potential mismatch in fusion images of planning computed tomography and follow-up MRI, the concordance coefficient (CC) was measured, and patients with a CC < 0.7 were excluded. Sixty patients were included. Multiple regression analysis was performed with the threshold dose as the objective variable and the age, dose, number of fractionations, Child-Pugh score, pretreatment liver volume, and pretreatment tumor volume as explanatory variables. The Student t test or Mann-Whitney U test was used as required.

Results: The median threshold doses for each number of dose fractionations (4 fractions, 12 fractions, and overall) were 51.6, 51.9, and 51.8 Gy (relative biological effectiveness [RBE]), respectively, in patients categorized as Child-Pugh class A and 27.0, 28.8, and 27.0 Gy (RBE), respectively, in patients categorized as Child-Pugh class B. In the multiple-regression analysis, only the Child-Pugh score was significant ($P < .001$). The number of dose fractionations was not statistically significant.

Conclusions: Although few patients in the study had decreased liver function, baseline liver function was the only factor significantly associated with the median threshold dose. These findings facilitate appropriate patient selection to receive C-ion RT for malignant hepatic tumors.

Sources of support: This study was supported with a grant to Gunma University from the program for Leading Graduate Schools, Cultivating Global Leaders in Heavy Ion Therapeutics and Engineering of the Ministry of Education, Culture, Sports, Science and Technology of Japan.

Disclosures: none.

*Corresponding author: Kei Shibuya, MD, PhD; E-mail: shibukei@gunma-u.ac.jp

https://doi.org/10.1016/j.adro.2021.100775

Introduction

The role of radiation therapy (RT) in the treatment of hepatocellular carcinoma has recently increased owing to improvements in high-precision irradiation technology.[1] Carbon-ion (C-ion) RT and proton therapy have excellent dose distributions. In particular, C-ion RT has a strong biological effect, regardless of the type of cancer cells.[2] Thus, C-ion RT for hepatic malignancies has achieved high local control rates comparable with those of other radical therapies such as radiofrequency ablation.[3-8] Gadoxetic acid (Gd-EOB-DTPA) is a contrast agent that is specifically taken up by hepatocytes via organic anion-transporting polypeptides (OATP1B3), and Gd-EOB-DTPA uptake may decrease in the presence of hepatocyte damage.[9,10] Therefore, the hepatobiliary phase (HBP) of Gd-EOB-DTPA–enhanced magnetic resonance imaging (MRI) can be used to evaluate liver function (besides providing detailed anatomic information) and is useful for predicting posthepatectomy liver function.[11-13] The irradiated hepatic area may suffer radiation-induced injury owing to vascular endothelial cell damage, with resultant hepatocyte damage.[14,15] Thus, we theorized that Gd-EOB-DTPA-enhanced MRI with high spatial resolution may be useful for the evaluation of radiation-induced liver disease.[16] Because the majority of primary liver tumors, especially hepatocellular carcinoma, may be associated with chronic liver disease, the prediction of post-RT liver function in hepatocellular carcinoma is important. It is equally important to ensure that the entire tumor and its margins are well within the irradiated area. In stereotactic body radiation therapy (SBRT) with x-ray and proton beam therapy, changes in the signal intensity of the HBP of Gd-EOB-DTPA-enhanced MRI and its threshold dose have been reported.[17,18]

The threshold dose of x-ray RT to the liver has been investigated; however, the threshold dose of the damaged liver tissue after C-ion RT remains unknown. C-ion beams have different effects from those of x-rays on irradiated cells. For example, C-ion RT has a greater tendency to cause DNA double-strand breaks than does x-ray RT.[19] Therefore, the cytotoxic effects of C-ion RT may differ even if the absorbed dose is equivalent to that of x-ray RT or gamma rays.[20,21]

To measure the effects of C-ion RT on the liver parenchyma, more information is needed. Therefore, this study aimed to obtain information about signal-intensity changes in Gd-EOB-DTPA-enhanced MRI in clinical cases. The primary endpoint of this study was to investigate the threshold dose of damaged hepatic tissue by observing the signal-intensity changes in the irradiated area after C-ion RT. The secondary endpoint was to identify factors that may affect the threshold dose.

Materials and Methods

Patient selection

This retrospective study enrolled patients who, after receiving C-ion RT, consecutively underwent their first 3-month follow-up MRI scan at our institution from April 2015 to March 2018 and who had undergone MRI of the upper abdomen within 1 month before commencing C-ion RT for malignant liver tumors. All patients were evaluated by Gd-EOB-DTPA–enhanced MRI before treatment except 1 patient who was treated for hepatocellular carcinoma for the first time and had good liver function. The follow-up interval was based on our institution's follow-up protocol.

Patients were excluded according to the following criteria: (1) they had a history of RT for the targeted tumor (patients whose target tumors were treated by methods other than RT were included), (2) they were imaged using MRI with magnetic field strength other than 3 Tesla, and/or (3) they had a concordance coefficient (CC), described later in the Methods and Materials, less than 0.7 (this was to evaluate potential mismatch in fusion images of planning computed tomography [CT] and follow-up MRI). Patients who met any of the exclusion criteria were excluded from all data analyses.

Tacit informed consent for this retrospective study was obtained through an opt-out notice posted on the institutional website, as approved by the ethics committee (Gunma University Hospital Clinical Research Review Board), and participants who communicated their refusal to participate were excluded from the study.

MRI acquisition and evaluation

We collected clinical and imaging data from the electronic medical records and picture archiving and communication system at the study center. Our hospital has 2 types of 3-Tesla MRI scanners (Prisma and Skyra; Siemens Healthineers, Erlangen, Germany). Sequences taken in all cases were as follows: axial 3-dimensional gradient echo (GR) Dixon T1-weighted images, axial 2-dimensional (2D) single-shot turbo spin echo T2-weighted images, axial and coronal 2D turbo spin echo fat-saturated T2-weighted images, axial 2D echo planner imaging diffusion-weighted images, and axial and

coronal (only HBP) Gd-EOB-DTPA-enhanced 4-phase dynamic and HBP images (imaging was done before and at 30 seconds, 60 seconds, 120 seconds, and 20 minutes after the injection of Gd-EOB-DTPA). Imaging conditions for dynamic and HBP images were as follows: slice thicknesses were 1.5 to 3 mm, repetition times were 2.97 to 3.14 milliseconds, echo times were 1.03 to 1.17 milliseconds, flip angles were 8.5° to 10°, horizontal pixels were 320 to 512, and vertical pixels were 230 to 384.

Treatment plan of C-ion RT

All patients underwent simulation and planning of C-ion RT based on respiratory-gated CT scanning. Patients were immobilized using moldable cushions (Moldcare, Alocare, Tokyo, Japan) and thermoplastic shells (Shellfitter, Kuraray, Co., Ltd., Osaka, Japan) during the simulation CT and C-ion RT. The gross tumor volume was defined on the fusion image of respiratory-gated CT with dynamic contrast-enhanced CT and/or Gd-EOB-DTPA-enhanced MRI. Treatment plans, including doses and fractionations, were generated by radiation oncologists at our institution.

The C-ion RT dose was calculated using the relative biological effectiveness (RBE) of 3 and was reported in Gy (RBE). The C-ion beam was generated in the synchrotron (Hitachi, Ltd, Tokyo, Japan) at our institution, and the energy of the C-ion beam was 290, 380, or 400 MeV, based on the depth of the tumor.[22] Treatment planning was performed using MIM Maestro (MIM Software Inc, Cleveland, Ohio), and the data collected and referenced in this study were the pretreatment liver volume, tumor volume, dose distribution, and dose-volume histogram (DVH).

Image analyses

The region that appeared to have been irradiated with C-ion beams was depicted as a low-signal-intensity area on HBP images owing to the locally impaired liver function (Fig 1). This postradiation area of signal change was defined as the focal liver reaction (FLR). We carefully outlined the liver, the targeted tumor, and the FLR on the HBP. Two radiologists (with 5 and 15 years of experience as radiologists, respectively) confirmed that the outlines were appropriate. The volume surrounded by the outlines was automatically calculated using MIM Maestro. If the tumor was difficult to identify on HBP images, other sequences from the same MRI examinations were used as references.

Measurement of the threshold dose and calculation of the CC

We measured the FLR volume on HBP and calculated a threshold dose by plotting it on a graph of the DVH of the whole liver. However, because the FLR volume measured by the HBP image also included the tumor volume, it was necessary to correct the change in tumor volume that resulted from treatment. Thus, we revised the FLR volume using the same method as in studies of SBRT.[17,23] Specifically, we calculated the corrected FLR (cFLR) by calculating the tumor's volume change from before to after the treatment (ie, the difference between the posttreatment tumor volume and the pretreatment tumor volume) and adding this to the FLR (cFLR = FLR + tumor volume change).

To evaluate potential mismatch in fusion images of planning CT and follow-up MRI, this study measured the CC and excluded patients with a CC less than 0.7 from statistical analysis. These methods were similar to those of a previously reported SBRT study.[17] The region irradiated with a dose beyond the threshold dose was defined as the highly irradiated area (HIA). The CC was the volume of the common area of the HIA and the FLR divided by the volume of the FLR. The HIA may have extended beyond the hepatic margins; however, HBP images could be used to accurately evaluate only the hepatic signal-intensity changes. Therefore, the CC was evaluated only for the liver. The CC was calculated as follows: (1) the

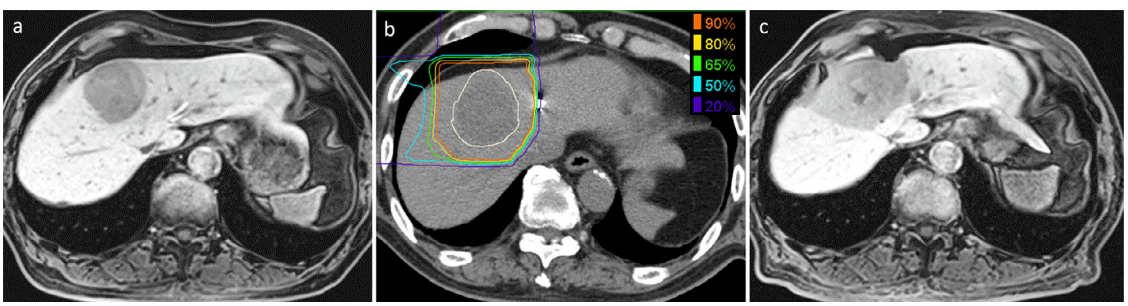

Fig. 1 Signal intensity changes of hepatobiliary phase (HBP) images of gadoxetic acid (Gd-EOB-DTPA)–enhanced magnetic resonance imaging (MRI) after C-ion radiation therapy. (A) HBP image of pretreatment Gd-EOB-DTPA-enhanced MRI; the tumor is visible as a hypointense mass in the right hepatic lobe (5.6 cm). (B) Planning computed tomography; gross tumor volume (white line) and isodose lines (orange, 90%; yellow, 80%; green, 65%; blue, 50%; purple, 20%) are shown. (C) HBP image of Gd-EOB-DTPA-enhanced MRI 3 months after treatment. The region that has been irradiated is observed to be a low-signal-intensity region.

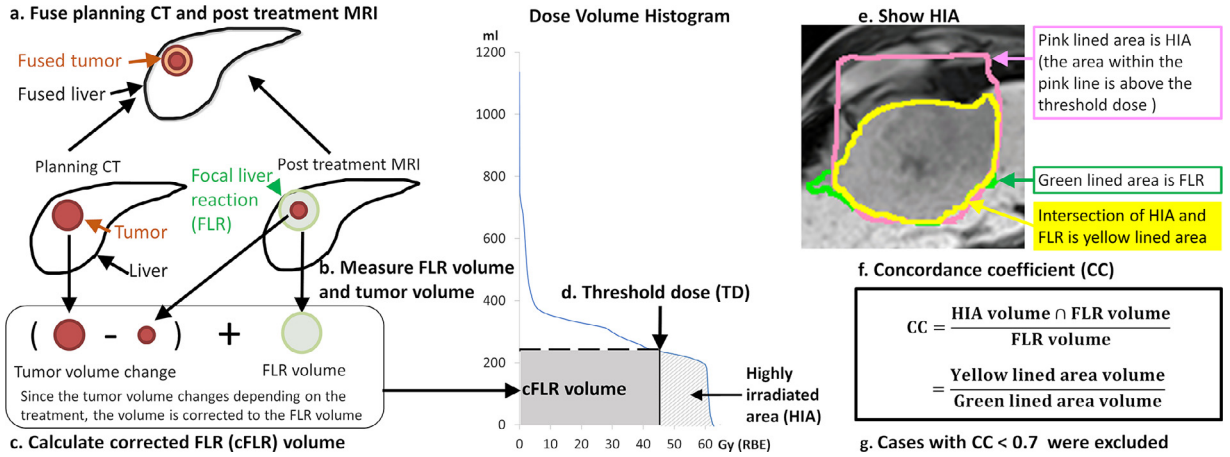

Fig. 2 Overall flow from the measurement of the threshold dose to the calculation of the concordance coefficient. The filled red circle indicates the tumor, the green circle indicates the focal liver reaction (FLR), the pink circle indicates the highly irradiated area (HIA), and the yellow area indicates an intersection of FLR and HIA. (A) Creation of a computed tomography−magnetic resonance imaging fusion image. (B) Measurement of the tumor volume and FLR volume. (C) Calculation of the tumor volume change before and after treatment and the addition of this volume to the FLR volume to calculate the corrected FLR (cFLR) volume. (D) Calculation of a threshold dose by including the cFLR in a graph of the dose-volume histogram of the whole liver. (E) The area above the threshold dose (HIA) is displayed on the fusion image. (F) The intersection of the FLR and HIA is clipped out, and the volume is measured and divided by the FLR volume. This value is the concordance coefficient (CC). (G) Cases with a CC < 0.7 were excluded.

FLR and HIA were displayed on the CT-MRI fusion image; (2) the intersecting volume of the FLR and the HIA in the liver was clipped out and measured; and (3) this volume was divided by the FLR volume to obtain the CC. Figure 2 shows the overall process flow from the measurement of the threshold dose to the calculation of the CC.

Statistical analyses

IBM SPSS, version 25 (IBM Corp, Armonk, New York) was used for statistical analyses. We performed a multiple-regression analysis in which the objective variable was the threshold dose and the explanatory variables were age, the dose, the number of fractionations of the C-ion RT, the Child-Pugh score,[24,25] the pretreatment liver volume, and the pretreatment tumor volume. Moreover, multicollinearity tests were conducted, and variables with a variance inflation factor of 10 or greater were excluded. A significance test (Student t test or Mann-Whitney U test) was performed as needed. Statistical significance was set at $P < .05$.

In this study, all patient information was anonymized before analyses. This study was approved by the ethics committee of our institution (Gunma University Hospital Clinical Research Review Board).

Results

The patient selection flowchart is shown in Figure 3. Of the 72 patients identified on screening, 12 (17%) who did not meet the eligibility criteria were excluded and 60 (83%) were included in the analysis. Five of the 12 excluded patients had a history of RT (all had received C-ion RT) or were followed up with 1.5T MRI, and the remaining 7 patients had a CC less than 0.7. Of these 7 excluded patients, we could not evaluate the FLR in 2 owing to poor Gd-EOB-DTPA uptake of the entire liver; 2 of the patients underwent transcatheter arterial chemoembolization (TACE) immediately before C-ion RT (within 2 months); 1 patient had biliary atresia owing to cholangiocarcinoma in the irradiated area; 1 patient was treated for multiple hepatocellular carcinomas of the right lobe at the same time; and a new metastatic lesion appeared at the border of the irradiation area in 1 patient. Characteristics of the study participants are summarized in Table 1. Most of the patients (85%) had chronic hepatitis, with hepatitis C virus infection being the most common etiology. The median interval from the completion of irradiation treatment to the MRI examination was 90 days (range, 71-120 days).

The results for the threshold doses classified by dose fractionation are shown in Table 2. For each number of dose fractionations (4 fractions, 12 fractions, and overall), the median threshold doses in patients categorized as Child-Pugh class A were 51.6, 51.9, and 51.8 Gy (RBE), respectively, whereas those in patients categorized as Child-Pugh class B were 27.0, 28.8, and 27.0 Gy (RBE), respectively. No significant difference was observed between the median number of dose fractionations (4 fractions, 51.0 Gy [RBE]; interquartile range [IQR], 36.2-56.6 Gy [RBE]; 12 fractions: 44.0 Gy [RBE]; IQR, 38.2-55.6 Gy [RBE]) combined for all Child-Pugh classes (P = .76, Mann-Whitney U test). When both

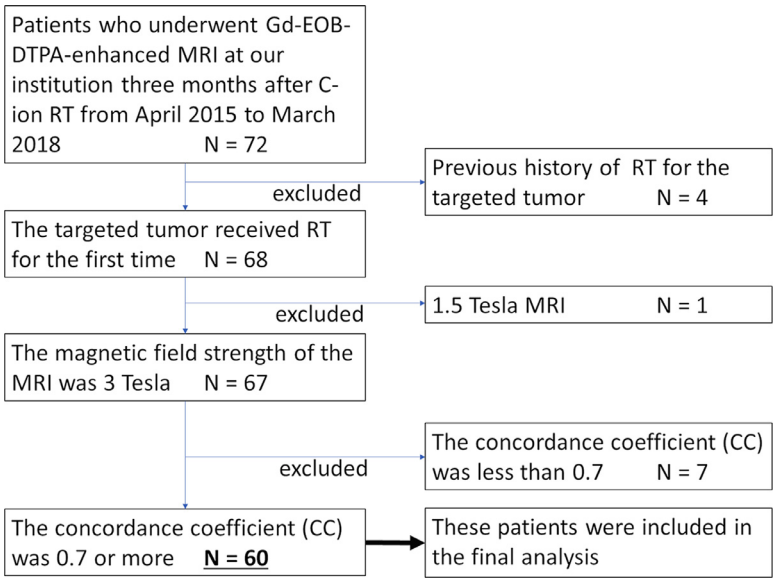

Fig. 3 Flowchart of the patient-selection study procedure.

fractionations were combined, the median threshold dose of Child-Pugh class B (27.0 Gy [RBE]; IQR, 24.0-32.8 Gy [RBE]) was significantly lower than that of Child-Pugh class A (51.8 Gy [RBE]; IQR, 40.2-56.6 Gy [RBE]) ($P < .001$, Mann-Whitney U test). One patient was categorized as Child-Pugh class C but showed a threshold dose of 16.1 Gy (RBE), which was much lower than that of patients in class A or B.

In the multiple-regression analysis, the only factor with significant differences was the Child-Pugh score ($P < .001$). No significant differences were observed in age ($P = .82$), dose ($P = .87$), number of dose fractionations ($P = .75$), pretreatment tumor volume ($P = .19$), or pretreatment liver volume ($P = .44$). The variance inflation factor was 1.5 or less for all variables. The relationship between the threshold doses for the Child-Pugh score is shown in Figure 4. The regression equation with the threshold dose as the objective variable and the Child-Pugh score as the explanatory variable is as follows:

$$\text{Threshold dose(Gy[RBE])} = -5.64 \times (\text{Child} - \text{Pugh score}) + 77.44$$

Discussion

In this study, the threshold doses in patients with a Child-Pugh class A grading were 51 to 52 Gy (RBE). Liver function was the only factor significantly associated with the threshold doses. In an SBRT study by Sanuki et al, the median threshold dose was reported to be 30.5 for patients with Child-Pugh class A grading and 25.2 Gy for patients with Child-Pugh class B grading.[17] In this study, the threshold doses of C-ion RT were substantially higher than those in the study by Sanuki et al: 51.8 Gy (RBE) for patients in Child-Pugh class A and 27.0 Gy (RBE) for patients in Child-Pugh class B.

Because C-ion RT has excellent dose distribution and reduces the volume of medium-to-low-dose areas compared with treatment with the same dose as in x-ray RT,[26] it may have enabled preservation of the function of the surrounding normal liver parenchyma, which in turn may have influenced the increase in the threshold dose. However, this difference between C-ion RT and x-rays was more likely owed to the difference in biological features because the threshold dose for proton beams (which have a dose distribution similar to that of C-ion RT but biological effectiveness similar to that of x-ray RT) was reported to be similar to that of x-ray RT.[18] Regarding the biological properties, double-strand DNA breaks are more likely to occur with C-ion beams than with x-rays, ensuring that the cytotoxic effect of C-ion beams is different from that of x-rays and gamma rays, even at the same dose.[19] The dose ratio for obtaining the same equivalent effect is called RBE.[21] The RBE of C-ion RT has been reported to be approximately 3 for cancer cells, based on experimental studies using various cell lines.[27-29] The clinical dose of C-ion RT is usually described in Gy (RBE), which is calculated by multiplying the C-ion absorbed dose by an RBE of 3, although the RBE of C-ions varies by the tissue type, cell proliferation ability, and oxygenation status.[30,31] Many factors may be involved in RBE, and RBE may differ between the normal liver parenchyma and tumor tissue. The RBE of C-ion RT for the liver parenchyma compared with that in an x-ray RT study[17] was estimated to be 1.77 for patients in Child-Pugh class A and 2.80 for patients in Child-Pugh class B. The RBE in the livers of mice was reported to be 1.86,[32] which is consistent with the results

Table 1 Patient characteristics

Characteristic	Patients, no. (%) (N = 60)*
Sex	
Male	37 (62)
Female	23 (38)
Age, median (range), y	7 (51-91)
Type of chronic hepatitis	
HBV infection	4 (7)
HCV infection	34 (57)
Alcoholic	4 (7)
Nonalcoholic steatohepatitis	7 (12)
Autoimmune	1 (2)
Primary biliary cholangitis	1 (2)
No hepatitis	9 (15)
Child-Pugh class	
A	55 (92)
B	4 (7)
C	1 (2)
Clinical diagnosis of tumor	
HCC	55 (92)
CCC	3 (5)
Metastasis	2 (3)
Treatment history of target lesion	
TACE	22 (37)
RFA	2 (3)
TACE + RFA	1 (2)
None	35 (58)
Treatment protocol	
52.8 Gy (RBE) / 4 fr	1 (2)
60.0 Gy (RBE) / 4 fr	40 (67)
60.0 Gy (RBE) / 12 fr	18 (30)
64.8 Gy (RBE) / 12 fr	1 (2)
Liver volume, median (IQR), mL	1047 (902-1250)
GTV, median (IQR), mL	24.4 (13.8-72.1)
Interval between C-ion radiation therapy and MRI, median (IQR), d	90 (85-94.5)

Abbreviations: C-ion = carbon ion; CCC = cholangiocellular carcinoma; GTV = gross tumor volume; HBV = hepatitis B virus; HCC = hepatocellular carcinoma; HCV = hepatitis C virus; IQR = interquartile range; MRI = magnetic resonance imaging; RBE = relative biological effectiveness; RFA = radiofrequency ablation; TACE = transcatheter arterial chemoembolization.

* Data are presented as number (percentage) of patients unless otherwise indicated.

of this study in patients with preserved liver function (Child-Pugh class A).

In this study, the Child-Pugh classification was the only factor significantly associated with the threshold dose, and the threshold dose decreased with the decline in liver function. The number of fractionations has been reported to be an important factor for the threshold dose in x-ray RT,[17,33,34] although no significant difference was observed for C-ion RT. Thus, high linear energy transfer radiation, such as C-ion beams, may be less affected by fractionated irradiation. Radiation-induced liver disease may be more likely to occur in patients with decreased liver function.[35,36] In this study, the threshold dose of C-ion RT for patients with a Child-Pugh class A grading was much higher than that for SBRT, whereas the threshold dose for patients with Child-Pugh class B grading was much lower and was more similar to that for SBRT.[17] In patients with Child-Pugh class A grading, it may be possible to take advantage of the high threshold dose to consider increasing the dose to improve local control. Also, the high threshold dose of C-ion RT means a smaller area of liver function loss compared with x-ray RT. This may be beneficial in the treatment of multiple lesions that tend to have a larger irradiation area. In patients with Child-Pugh class B grading, the RBE for the tumor and the liver parenchyma is similar, so it may be necessary to pay attention to the C-ion irradiation area as well as x-ray RT.

In this study, the irradiated area was depicted as a low-signal-intensity region on the HBP of Gd-EOB-DTPA-enhanced MRI. There are several reports of HBP images being used to evaluate irradiation areas treated with x-rays, gamma rays, and proton beams.[16-18,33,34,37-41] There are 2 methods for determining the threshold dose. One method involves the application of the FLR volume of the posttreatment MRI to the DVH of the planning CT, as was done in this study.[17,18,40] Another method is to visually or numerically evaluate the posttreatment MRI and compare it with the planning CT.[16,33,34,37-39,41] We did not use the latter method, owing to the unexpected distortion in the fusion images. This study was conducted using almost the same method as that used in the SBRT study by Sanuki et al,[17] and the use of DVH was suspected to be less affected by the performance of the software for nonrigid fusion images. The liver volume may change after C-ion RT,[42] and we occasionally observed deformation of the liver after treatment. Our method did not consider liver deformation after radiation therapy; however, the FLR and HIA were generally concordant, except in cases with poor Gd-EOB-DTPA uptake, TACE immediately before C-ion RT, biliary complications, multiple lesions, and new metastasis. Therefore, we inferred that our method was sufficiently valid to evaluate the irradiated area in C-ion RT.

This study has limitations. First, there was relatively large variation in the threshold dose for the same Child-Pugh score. The Child-Pugh score is a semiquantitative score; therefore, there was a wide range of liver function among the study participants, even if they had the same scores. This may have been the cause of the variability in the threshold dose. However, the Child-Pugh classification is the most widely accepted classification for evaluating liver function in the treatment of liver cancer.[43] Second, only 5 patients had a grading of Child-Pugh class B or C. Therefore, there was a significant difference in the threshold dose depending on liver function, but it may not have been accurate. Third, the treatment protocols for C-ion RT

Table 2 Threshold doses and concordance coefficients

Child-Pugh class	Threshold dose, Gy (RBE)					
	Four fractions (n = 41)		Twelve fractions (n = 19)		Total (N = 60)	
	Median	IQR	Median	IQR	Median	IQR
A (n = 55)	51.6	40.4-56.7	51.9	39.5-56.5	51.8	40.2-56.6
B (n = 4)	27.0	-	28.8	-	27.0	24.0-32.8
C (n = 1)	16.1	-	-	-	16.1	-
Total	51.0	36.2-56.5	44.0	38.2-55.6	50.1	37.7-56.2
Concordance coefficient	0.81	0.74-0.89	0.84	0.76-0.91	0.81	0.75-0.90

Abbreviations: IQR = interquartile range; RBE = relative biological effectiveness.

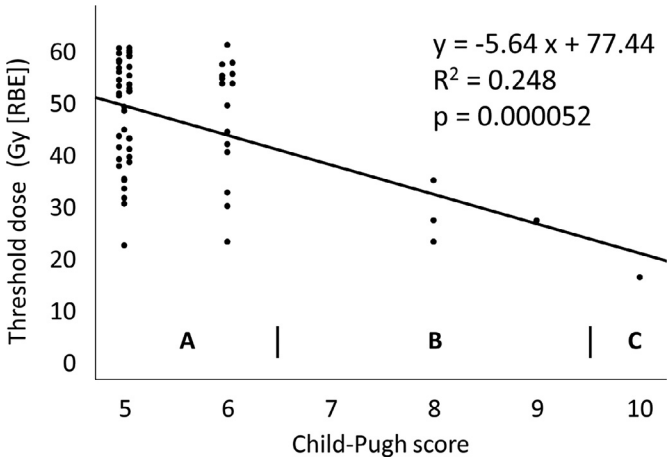

Fig. 4 Scatter diagram of the threshold dose according to the Child-Pugh score. A, B, and C in the figure represent the Child-Pugh classification. *Abbreviation:* RBE = relative biological effectiveness.

were not uniform, although the effect of the number of fractionations on RBE was not significant.[2] Regarding the linear quadratic model, we expected that high linear energy transfer radiation, such as C-ion beams, would be less dependent on dose fractionation than are x-rays. To address these limitations in future studies, the accuracy of the threshold dose in patients with impaired liver function can be improved by increasing the number of patients. Furthermore, we hope to identify quantitative indicators of liver function that can reflect the threshold dose more accurately than the Child-Pugh score.

Conclusion

The median threshold doses for Child-Pugh class A and B patients were 51.8 and 27.0 Gy (RBE). In this study, for patients with a Child-Pugh class A grading, C-ion RT showed a higher threshold dose compared with x-ray RT. Although patients with decreased liver function were few, baseline liver function was the only significant factor that affected the threshold dose. These results provide useful information for appropriate selection of patients to receive C-ion RT for malignant hepatic tumors.

Acknowledgments

We thank Editage for English language editing.

References

1. Bang A, Dawson LA. Radiotherapy for HCC: Ready for prime time? *JHEP Rep*. 2019;1:131–137.
2. Karger CP, Peschke P. RBE and related modeling in carbon-ion therapy. *Phys Med Biol*. 2017;63:01TR02.
3. Imada H, Kato H, Yasuda S, et al. Comparison of efficacy and toxicity of short-course carbon ion radiotherapy for hepatocellular carcinoma depending on their proximity to the porta hepatis. *Radiother Oncol*. 2010;96:231–235.
4. Kondo Y, Kimura O, Shimosegawa T. Radiation therapy has been shown to be adaptable for various stages of hepatocellular carcinoma. *World J Gastroenterol*. 2015;21:94–101.
5. Izzo F, Granata V, Grassi R, et al. Radiofrequency ablation and microwave ablation in liver tumors: An update. *Oncologist*. 2019;24:e990–e1005.
6. Komatsu S, Fukumoto T, Demizu Y, et al. Clinical results and risk factors of proton and carbon ion therapy for hepatocellular carcinoma. *Cancer*. 2011;117:4890–4904.
7. Shibuya K, Ohno T, Terashima K, et al. Short-course carbon-ion radiotherapy for hepatocellular carcinoma: A multi-institutional retrospective study. *Liver Int*. 2018;38:2239–2247.

8. Kasuya G, Kato H, Yasuda S, et al. Progressive hypofractionated carbon-ion radiotherapy for hepatocellular carcinoma: Combined analyses of 2 prospective trials. *Cancer*. 2017;123:3955–3965.
9. Narita M, Hatano E, Arizono S, et al. Expression of OATP1B3 determines uptake of Gd-EOB-DTPA in hepatocellular carcinoma. *J Gastroenterol*. 2009;44:793–798.
10. Motosugi U, Ichikawa T, Sou H, et al. Liver parenchymal enhancement of hepatocyte-phase images in Gd-EOB-DTPA-enhanced MR imaging: Which biological markers of the liver function affect the enhancement? *J Magn Reson Imaging*. 2009;30:1042–1046.
11. Chuang YH, Ou HY, Lazo MZ, et al. Predicting post-hepatectomy liver failure by combined volumetric, functional MR image and laboratory analysis. *Liver Int*. 2018;38:868–874.
12. Asenbaum U, Kaczirek K, Ba-Ssalamah A, et al. Post-hepatectomy liver failure after major hepatic surgery: Not only size matters. *Eur Radiol*. 2018;28:4748–4756.
13. Araki K, Harimoto N, Yamanaka T, et al. Efficiency of regional functional liver volume assessment using Gd-EOB-DTPA-enhanced magnetic resonance imaging for hepatocellular carcinoma with portal vein tumor thrombus. *Surg Today*. 2020;50:1496–1506.
14. Reed Jr GB, Cox Jr. AJ. The human liver after radiation injury. A form of veno-occlusive disease. *Am J Pathol*. 1966;48:597–611.
15. Takamatsu S, Kozaka K, Kobayashi S, et al. Pathology and images of radiation-induced hepatitis: A review article. *Jpn J Radiol*. 2018;36:241–256.
16. Sun XL, Jiang X, Kuang Y, et al. Potential of Gd-EOB-DTPA as an imaging biomarker for liver injury estimation after radiation therapy. *Hepatobiliary Pancreat Dis Int*. 2019;18:354–359.
17. Sanuki N, Takeda A, Oku Y, et al. Threshold doses for focal liver reaction after stereotactic ablative body radiation therapy for small hepatocellular carcinoma depend on liver function: Evaluation on magnetic resonance imaging with Gd-EOB-DTPA. *Int J Radiat Oncol Biol Phys*. 2014;88:306–311.
18. Takamatsu S, Yamamoto K, Maeda Y, et al. Evaluation of focal liver reaction after proton beam therapy for hepatocellular carcinoma examined using Gd-EOB-DTPA enhanced hepatic magnetic resonance imaging. *PLoS One*. 2016;11: e0167155.
19. Oike T, Niimi A, Okonogi N, et al. Visualization of complex DNA double-strand breaks in a tumor treated with carbon ion radiotherapy. *Sci Rep*. 2016;6:22275.
20. Suzuki M, Kase Y, Yamaguchi H, et al. Relative biological effectiveness for cell-killing effect on various human cell lines irradiated with heavy-ion medical accelerator in Chiba (HIMAC) carbon-ion beams. *Int J Radiat Oncol Biol Phys*. 2000;48:241–250.
21. Schardt D, Elsässer T, Schulz-Ertner D. Heavy-ion tumor therapy: Physical and radiobiological benefits. *Rev Mod Phys*. 2010;82:383–425.
22. Ohno T, Kanai T, Yamada S, et al. Carbon ion radiotherapy at the Gunma University Heavy Ion Medical Center: new facility set-up. *Cancers (Basel)*. 2011;3:4046–4060.
23. Takeda A, Oku Y, Sanuki N, et al. Dose volume histogram analysis of focal liver reaction in follow-up multiphasic CT following stereotactic body radiotherapy for small hepatocellular carcinoma. *Radiother Oncol*. 2012;104:374–378.
24. Child CG, Turcotte JG. Surgery and portal hypertension. *Major Probl Clin Surg*. 1964;1:1–85.
25. Pugh RN, Murray-Lyon IM, Dawson JL, et al. Transection of the oesophagus for bleeding oesophageal varices. *Br J Surg*. 1973;60:646–649.
26. Abe T, Saitoh J, Kobayashi D, et al. Dosimetric comparison of carbon ion radiotherapy and stereotactic body radiotherapy with photon beams for the treatment of hepatocellular carcinoma. *Radiat Oncol*. 2015;10:187.
27. Jianshe Y, Wenjian L, Xiaodong J, et al. Survival and initial chromatid breakage in normal and tumour cells exposed in vitro to gamma rays and carbon ions at the HIRFL. *Br J Radiol*. 2006;79:518–521.
28. Cui X, Oonishi K, Tsujii H, et al. Effects of carbon ion beam on putative colon cancer stem cells and its comparison with X-rays. *Cancer Res*. 2011;71:3676–3687.
29. Oonishi K, Cui X, Hirakawa H, et al. Different effects of carbon ion beams and X-rays on clonogenic survival and DNA repair in human pancreatic cancer stem-like cells. *Radiother Oncol*. 2012;105:258–265.
30. Tinganelli W, Ma NY, Von Neubeck C, et al. Influence of acute hypoxia and radiation quality on cell survival. *J Radiat Res*. 2013;54(Suppl 1):i23–i30.
31. Calipel A, Lux AL, Guerin S, et al. Differential radiosensitivity of uveal melanoma cell lines after x-rays or carbon ions radiation. *Invest Ophthalmol Vis Sci*. 2015;56:3085–3094.
32. Tomizawa M, Miyamoto T, Kato H, et al. Relative biological effectiveness of carbon ions for causing fatal liver failure after partial hepatectomy in mice. *J Radiat Res*. 2000;41:151–161.
33. Jung J, Yoon SM, Cho B, et al. Hepatic reaction dose for parenchymal changes on Gd-EOB-DTPA-enhanced magnetic resonance images after stereotactic body radiation therapy for hepatocellular carcinoma. *J Med Imaging Radiat Oncol*. 2016;60:96–101.
34. Fukugawa Y, Namimoto T, Toya R, et al. Radiation-induced liver injury after 3D-conformal radiotherapy for hepatocellular carcinoma: Quantitative assessment using Gd-EOB-DTPA-enhanced MRI. *Acta Med Okayama*. 2017;71:25–29.
35. Xu ZY, Liang SX, Zhu J, et al. Prediction of radiation-induced liver disease by Lyman normal-tissue complication probability model in three-dimensional conformal radiation therapy for primary liver carcinoma. *Int J Radiat Oncol Biol Phys*. 2006;65:189–195.
36. Jung J, Yoon SM, Kim SY, et al. Radiation-induced liver disease after stereotactic body radiotherapy for small hepatocellular carcinoma: Clinical and dose-volumetric parameters. *Radiat Oncol*. 2013;8:249.
37. Jung SH, Yu JI, Park HC, et al. A feasibility study evaluating the relationship between dose and focal liver reaction in stereotactic ablative radiotherapy for liver cancer based on intensity change of Gd-EOB-DTPA-enhanced magnetic resonance images. *Radiat Oncol J*. 2016;34:64–75.
38. Nakamura Y, Kimura T, Higaki T, et al. Clinical utility of gadoxetate disodium-enhanced hepatic MRI for stereotactic body radiotherapy of hepatocellular carcinoma. *Jpn J Radiol*. 2015;33:627–635.
39. Okamoto D, Nishie A, Asayama Y, et al. Gadolinium ethoxybenzyl diethylenetriamine pentaacetic acid-enhanced MR finding of radiation-induced hepatic injury: Relationship to absorbed dose and time course after irradiation. *Magn Reson Imaging*. 2014;32:660–664.
40. Seidensticker M, Seidensticker R, Mohnike K, et al. Quantitative in vivo assessment of radiation injury of the liver using Gd-EOB-DTPA enhanced MRI: Tolerance dose of small liver volumes. *Radiat Oncol*. 2011;6:40.
41. Richter C, Andronesi OC, Borra RJH, et al. Inter-patient variations of radiation-induced normal-tissue changes in Gd-EOB-DTPA-enhanced hepatic MRI scans during fractionated proton therapy. *Clin Transl Radiat Oncol*. 2019;18:113–119.
42. Imada H, Kato H, Yasuda S, et al. Compensatory enlargement of the liver after treatment of hepatocellular carcinoma with carbon ion radiotherapy—Relation to prognosis and liver function. *Radiother Oncol*. 2010;96:236–242.
43. Forner A, Reig M, Bruix J. Hepatocellular carcinoma. *Lancet*. 2018;391:1301–1314.